Magnetic Resonance in Medicine 56:717–725 (2006)

Enhanced T_2 Contrast for MR Histology of the Mouse Brain

Anjum Ali Sharief[1] and G. Allan Johnson[1*]

A 3D Carr-Purcell-Meiboom-Gill (CPMG) sequence was implemented to obtain enhanced T_2 contrast in actively stained (perfusion with fixative and contrast agent) mouse brains at 9.4 T. Short interecho spacing was used to minimize diffusion and susceptibility losses. The sequence produced 16 3D volumes with an interecho spacing of 7 ms for isotropic 43-μ-resolution images of the mouse brains in a scan time of 4 hr. To enhance the signal-to-noise ratio (SNR) and contrast, the multiecho frequency domain image contrast (MEFIC) method was applied, resulting in a composite image with T_2-weighted contrast. The high SNR and contrast thus achieved revealed aspects of mouse brain morphology, such as multiple cortical layers, groups of thalamic nuclei, layers of the inferior and superior colliculus, and molecular and granular layers of the cerebellum, with a high degree of definition and contrast that was not previously achieved in T_2-weighted acquisitions at high fields. Magn Reson Med 56:717–725, 2006. © 2006 Wiley-Liss, Inc.

Key words: mouse brain; magnetic resonance histology; MEFIC; 3D-CPMG; T_2

Magnetic resonance histology (MRH) (1) has become a vital tool for a wide range of applications in pathology, neurobiology, and developmental biology. The use of superconducting magnets at high field strengths, specialized RF coils, and fast switching gradients has enabled resolution of ≥50 μ in the rodent brain (2,3). MRH offers an attractive complement to conventional histology, which is labor- and time-intensive. 3D images from MRH allow sectioning to be performed along any plane without the need for alignment and matching. The high soft-tissue contrast and signal-to-noise ratio (SNR) that it provides in the brain makes MRH particularly appealing for our specific application, i.e., morphometry in the mouse brain. Neuromorphometry includes volumetric analysis, shape information, and spatial organization of structures, which form the basis of morphological phenotyping of mouse models.

A prerequisite for morphometry studies in the brain, however, is the ability to visually discriminate one structure from another. MRH exploits the inherent tissue properties of proton density, diffusion, spin-lattice relaxation (T_1), and spin-spin relaxation (T_2) to emphasize differences among tissue types and indicate the presence of pathology. An accurate assessment of these properties at high fields can guide the selection of scan parameters for maximum differential contrast of structures in the rodent brain. The high magnetic field strengths used in MRH ensure an SNR increase by a power in the range of 1–1.75 of the magnetic field strength (4). However, an image-quality metric of greater utility in the differentiation of tissues is the contrast-to-noise ratio (CNR) (5,6). The CNR in MRI is driven by tissue properties of T_1, T_2, proton density, and diffusion. However, the behavior of these properties at high magnetic fields makes it difficult to achieve optimal contrast between tissues. Previous studies (7–9) showed an increase in tissue T_1s and a decrease in tissue T_2s as the strength of the magnetic field increased. The long T_1s necessitate inordinately long repetition times (TRs) to obtain truly T_2-weighted images that are independent of T_1. More significantly, diffusion through microscopic field gradients induced by tissue susceptibility differences results in much shorter T_2s compared to lower field strengths (9). Signal attenuation due to diffusion scales quadratically with the effective gradients (10), including susceptibility-induced and static field inhomogeneities. Susceptibility-induced inhomogeneities have a larger effect because they are spread over local regions, as opposed to static field inhomogeneities, which are essentially long-range field disturbances. Most static field inhomogeneities can be refocused by spin-echo techniques, but diffusion losses through susceptibility gradients are irreversible. Both static field and susceptibility inhomogeneities scale linearly with the magnetic field strength. In addition, imaging gradients in MRH reach values of 100–1000 mT/m, resulting in transverse relaxation and signal attenuation. Thus, it is challenging to obtain T_2-weighted contrast at microscopic dimensions and high fields.

Cremillieux et al. (11) reported one of the earliest studies for T_2 measurement in the rat brain at 7 T. T_2 measurements in the mouse brain were also obtained at 7 T in a study in which multiple acquisitions of a single-echo, multislice Carr-Purcell-Meiboom-Gill (CPMG) sequence were used to acquire images at six different TEs with a minimum TE of 15 ms (12). Multislice, multiecho acquisitions have been used as well (13); however, these can suffer from low SNR and artifacts at slice edges due to slice-selective refocusing pulses. The applications of such studies in rodents have ranged from quantitative T_2 analysis in cerebral ischemia (14), lesions of multiple sclerosis (15), and age-dependent T_2 differences (12). T_2-weighted contrast has found application in mouse models of Alzheimer's disease for detecting amyloid plaques (16) and assessing morphometric differences in the dentate gyrus (17). A 3D atlas of the mouse brain (18) provided average and variability measures for structures labeled on T_2-weighted data. 3D sequences with volume excitation are more suitable for high-field MRH because they compensate

Center for In Vivo Microscopy, Duke University Medical Center, Durham, North Carolina, USA.

Grant sponsor: National Institutes of Health (NIH)/National Center for Research Resources; Grant number: P41 RR 005959; NIH/National Cancer Institute (NCI); Grant number: R24 CA 092656.

*Correspondence to: G. Allan Johnson, Center for In Vivo Microscopy, Duke University Medical Center, Box 3302, Durham, NC 27710. E-mail: gaj@orion.duhs.duke.edu

Received 1 November 2005; revised 20 June 2006; accepted 23 June 2006.
DOI 10.1002/mrm.21026
Published online 8 September 2006 in Wiley InterScience (www.interscience.wiley.com).

for the loss of signal per voxel. Kovacevic et al. (18) used a 3D T_2-weighted sequence that achieved isotropic 60-μ resolution in 18.5 hr. Zhang et al. (16) used multiple 3D sequences at different TEs to yield a resolution of 46 × 46 × 62 μ in 24 hr. The 3D CPMG sequence used in this work is capable of much shorter TEs, higher resolution, and shorter acquisition times than the sequences used in the above-mentioned studies.

In a previous work (19) we outlined a multispectral MR acquisition protocol and algorithm for automated segmentation in the formalin-fixed mouse brain. Although the segmentation results were convincing, the long T_1 (~800 ms) in the mouse brain at 9.4 T required unreasonably long acquisition times. Johnson et al. (2) showed that the use of T_1-reducing contrast agents in conjunction with careful tissue fixation produces a fivefold increase in SNR and much shorter requirements for acquisition times. This enables higher resolution, which in turn makes detailed neuroanatomy visible at high fields. Unfortunately, the susceptibility variations induced by paramagnetic relaxation compounds reduce tissue T_2s, which makes differentiable T_2-weighted contrast a challenge at high fields. This work demonstrates the efficacy of a 3D CPMG acquisition and the multiecho frequency domain image contrast (MEFIC) method (20) for obtaining T_2-weighted images of actively stained mouse brain with high SNR and CNR. Though this method shows promise, to the best of our knowledge few studies have investigated its application. The initial study applied the technique to vasogenic edema and functional MRI (fMRI) studies in rats, both conducted at 3 T. We demonstrate the utility of this technique for high-field MRH in a focused study of the C57BL6/J mouse brain. The result is an accentuated visualization of mouse brain neuroanatomy.

THEORY

The CPMG sequence (21,22) is a reliable method for measuring T_2 relaxation times in tissues and in turn obtaining T_2-weighted images. The sequence consists of a single 90° RF excitation pulse followed by a train of 180° refocusing RF pulses. The signal decay in the CPMG sequence is a function of the TE and the T_2 relaxation time of the tissue. The signal at time TE can be written as

$$S(TE) \propto e^{(-TE/T_2)} \quad [1]$$

Due to the use of large gradients in MR microscopy and the induced susceptibility gradients at high fields, diffusion dominates at high fields. The functional dependence in Eq. [1] now becomes

$$S(TE) \propto e^{[(-TE/T_2)+(-TE/T_{2diff})]} \quad [2]$$

where

$$\frac{1}{T_{2diff}} = \frac{1}{12} G_{eff}^2 \gamma^2 D\ TE^2 \quad [3]$$

(10,23) G_{eff} is the effective gradient at a time TE arising due to imaging and susceptibility differences, and D is the diffusion constant. For water $D = 2.2 \times 10^{-5}$ cm^2/s. The measured T_2 relaxation time is then

$$\frac{1}{T_{2eff}} = \frac{1}{T_2} + \frac{1}{12} G_{eff}^2 \gamma^2 D\ TE^2 \ (4) \quad [4]$$

As a result, measured T_2s are shorter than expected. Clearly, reduction of TE can have a major impact on increasing T_{2eff}.

The CPMG sequence is highly sensitive to timing and RF pulse imperfections (24,25). Imperfect RF pulses and timing inconsistencies can lead to the formation of spurious echoes. Two kinds of artifacts plague multiecho sequences: a sinusoidal interference pattern along the phase-encoding axis, and mirror images from stimulated echoes superimposed on the data from the primary spin echoes. For 3D volume imaging the entire volume is excited per TR. The intensity variations in this case can also occur along the second phase-encoding axis, resulting in a banding artifact in the slice direction. Previous studies demonstrated the use of phase rewinding (26) and balanced crusher gradients (25,27) to eliminate these artifacts for 2D acquisitions. In this work we accordingly implemented crusher, encoding, and rewinding gradients for artifact removal in 3D CPMG acquisitions.

Conventionally, the later echoes in a multiecho acquisition are used to obtain T_2-weighted contrast between tissues. Although the longer TEs accentuate contrast differences between regions based on their different T_2 relaxation rates, the longer TEs also suffer from a lower SNR, which makes it difficult to identify and delineate structure boundaries. An innovative technique that has been shown to retain the SNR along with the T_2-weighted contrast is the MEFIC method (20). This approach computes the Fourier transform (FT) at each voxel of the echo images along the temporal dimension. The FT effectively integrates under the curve with tissues with longer T_2 time constants, producing higher and sharper peaks. The short tissue T_2's produce lower and broader peaks. Intensity differences in the DC image of the set thus arise due to T_2 relaxation differences, and this image has the maximum T_2-weighted contrast. Since the integration averages *k*-space data from all of the echo images, this image also has improved SNR. Along with the gain in signal and contrast, the MEFIC method optimizes the contrast among all of the tissue types that have different T_2 values, as opposed to conventional methods that generate the maximum contrast for a particular selection of tissue types at a particular TE value.

MATERIALS AND METHODS

Animal/Specimen Preparation

All of the animal studies were approved by the Duke University Institutional Animal Care and Use Committee. Six C57BL6/J male mice (approximately 9 weeks old) were used in the study. Two mice were fixed with formalin only, and four were fixed with a formalin and ProHance® (gadoteridol; Bracco Diagnostics, Inc., Princeton, NJ, USA) mixture. For the formalin fixation, the animals were transcardially perfused with an initial flush of 36 ml of 0.9% NaCl (37°C), followed by 36 ml of 10% buffered formalin.

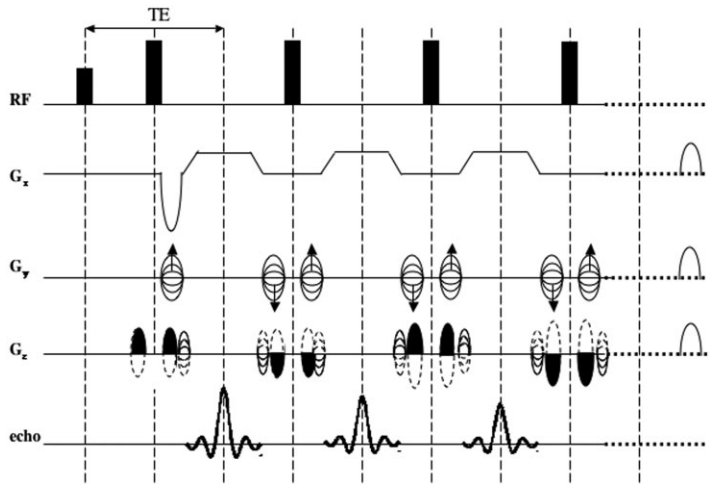

FIG. 1. 3D phase-encoded CPMG pulse sequence shows the RF pulses, G_x = readout gradient, G_y = phase-encoding gradient, G_z = slice-encoding gradient, and resultant echo train. The slice-encoding gradients and rewinding gradients are combined with the crusher gradients preceding and following the refocusing pulses, respectively. The solid and dashed lines of the slice-encoding gradient indicate polarity for a current repetition period.

The heads were then stored overnight in formalin. The brains were excised the next day and scanned. The remaining four mice were perfused using a transcardial approach with an initial flush of saline and 10% ProHance. This was followed by a mixture of 10% buffered ProHance solution in 10% buffered formalin to reduce tissue T_1. The mouse heads were stored in the mixture overnight and scanned within 24 hr. The brains were scanned in the skull. Care was taken to trim the skull to minimize post-processing required for skull stripping.

Pulse Sequence Implementation

The fixed specimens were imaged on a 9.4 T (400 MHz) vertical-bore Oxford magnet with a GE EXCITE console (Epic 11.0 GE Healthcare, Milwaukee, WI, USA). A 14-mm-diameter solenoid RF coil was used for the ex vivo, in situ mouse brains. The shielded gradients on the system are capable of peak strength of 850 mT/m with a rise time of 100 μs.

Figure 1 shows a schematic of the pulse sequence for a single TR. A single nonselective 90° RF pulse was used to excite the entire volume, followed by a train of 16 composite (28) $90°_x$-$180°_y$-$90°_x$ refocusing pulses. Composite pulses are used to improve both the inversion and refocusing efficiency of 180° pulses. 3D volume encoding was accomplished by stepping through successive phase-encoding gradients on two axes. The two phase-encoding gradients were applied after each refocusing pulse and rewound after the echo readout. Since stimulated echoes affected the later echoes more drastically and necessitated the use of higher crusher gradients, a pattern similar to the increasing crusher pattern (25) was used along the echo train. A constant phase difference was maintained between consecutive crushers. To make the gradients symmetrical on each side of the refocusing pulse, opposite halves of *k*-space were encoded in the odd and even echoes. This balanced both the crusher gradients and the encoding gradients around each refocusing pulse. To minimize the interecho spacing, the slice-encoding gradients and rewinding gradients were combined with the crusher preceding and following the refocusing pulses, respectively. Figure 1 illustrates the RF pulses, encoding waveforms on the *X*, *Y*, and *Z* gradients, and the resultant echo train. The solid and dashed lines of the waveforms on the slice-encoding gradient indicate polarity for a current repetition period. Killer gradients were placed on all three axes at the end of every cycle of TR to dephase all remaining magnetization.

Acquisition Protocol

Three sets of acquisition parameters were used for the brains actively stained with ProHance, and one set was used for the formalin-fixed brains. The three sets were used to gauge the impact of different TEs on the T_2 measurements in the actively stained brain. The parameters for the actively stained brain were significantly different from those used for the formalin-fixed brain to accommodate the different T_1s and T_2s of the specimens. Acquisition parameters for the formalin-fixed brains were TR = 1.8 s, interecho spacing = 10 ms, TE_{max} = 80 ms (eight echoes), with a resolution of 43 × 43 × 86 μ and a total scan time of 16 hr. For the actively stained mouse brain, all sets were acquired over a field of view (FOV) of 11 mm × 11 mm × 22 mm. For the first set the acquisition parameters included array dimensions of 128 × 128 × 128 (86 × 86 × 176 μ) with an interecho spacing of 4 ms and TE_{max} = 64 ms (16 echoes). However, although this was a low-resolution scan, it achieved the shortest interecho spacing. The second set, which had array dimensions of 256 × 256 × 256 (43 × 43 × 86 μ) with an interecho spacing of 5 ms and TE_{max} = 80 ms (16 echoes), was used for contrast analysis of the different images generated by the MEFIC method. The third set, which had dimensions of 256 × 256 × 512 (43 × 43 × 43 μ) with an interecho spacing of 7 ms and TE_{max} = 112 ms (16 echoes), was a high-resolution isotropic data set and was used for detailed structure identification. All acquisitions were 3D volume acquisitions using a bandwidth of 62.5 kHz and maximum crusher gradient amplitude of 80 mT/m. The minimum TE increased for the high-resolution data set, since we encoded the longer axis of the brain along the readout gradient.

For the isotropic high-resolution data set, we reduced the total acquisition time by limiting the acquisition to 75% of the full Nyquist sample along each of the two

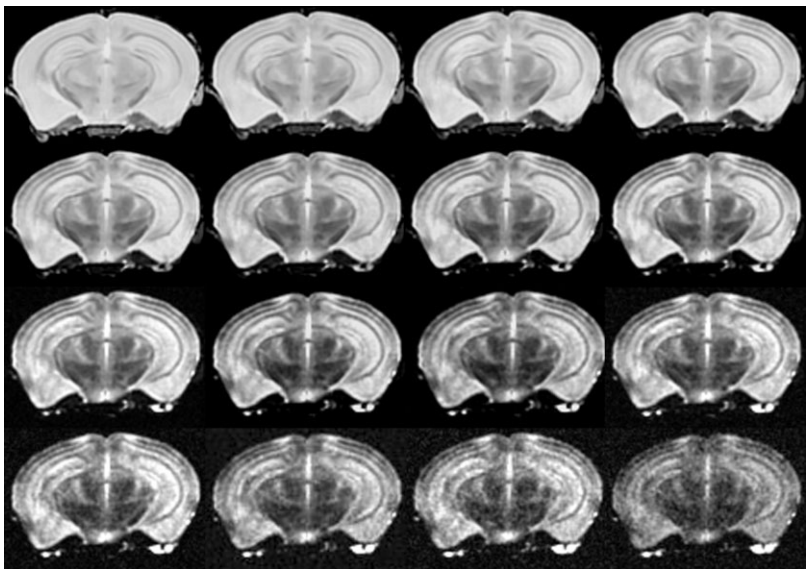

FIG. 2. Spin-echo images of a slice from a 3D CPMG volume acquisition (FOV = 11 × 11 × 22 mm, matrix = 128 × 128 × 128, TR = 400 ms, TE = 4, 8, 12. . .64 ms) show increasing T_2 contrast and decreasing SNR.

phase-encoding axes. This data set was acquired with a single NEX in a scan time of 4 hr. The remaining volume of *k*-space was zero-filled and an asymmetrically apodized Fermi filter was applied before reconstruction. A 3D FT was then applied to the data, which were displayed as magnitude images on a 3D array. In addition, we used a strategy designed to expand the dynamic range of the digitizer beyond 16 bits. The 3D volume of Fourier space was divided into three to six concentric volumes surrounding the center of *k*-space. We externally increased the receiver gain systematically for annuli away from the center of *k*-space, and reduced it for annuli toward the center by changing the number of attenuators used in the analog receiver. The increased gain at the periphery optimized the dynamic range of the receiver at the edges of *k*-space that encode high-frequency information.

Analysis

T_2 measurements were performed on all six brains. 3D multiecho data were fitted pixel by pixel with a nonlinear least-squares exponential decay function to derive T_2 estimates for the entire brain. These estimates were computed for the formalin-fixed brain for TE = 10 ms, and for the actively stained brain using the three different acquisition parameters corresponding to TE = 4, 5, and 7 ms. Regions of interest (ROIs) were placed in areas of gray matter (GM), white matter (WM), and cerebrospinal fluid (CSF). Using the 3D echo image sets, we computed a complex FT at each voxel along the echo dimension to generate the T_2-weighted image set with the MEFIC method (20). The CNR was also computed to compare between the resultant MEFIC image of the formalin-fixed and actively-stained brains. To test the efficacy of the frequency domain method, we evaluated the relative SNR, contrast, and CNR measurements among different sources of T_2-weighted images: a single-echo volume acquisition at a long TE that indicated T_2-weighted contrast, the eighth-echo volume from a 3D multiecho acquisition at the same TE as the first but with shorter interecho spacing, and a set of different MEFIC images using the last eight, last 14, last 15, and all 16 echoes in the computation of the T_2-weighted MEFIC image. These are labeled MEFIC-8, MEFIC-14, MEFIC-15, and MEFIC-16, respectively. This analysis was done on all four brains fixed with ProHance and using the second set of acquisition parameters.

We used the most common method for measuring the SNR in MR images, i.e., we determined the ratio of the mean signal in the area of interest to the standard deviation (SD) of the noise in the background:

$$SNR = \left(\frac{signal}{\sigma_{noise}} \right) \quad [5]$$

This measure differs from a true SNR primarily because of the magnitude reconstruction of the images and the dynamic receiver gain. The equation suffices in our case because we are reporting a relative SNR measure to indicate the quality of the different T_2-weighted MEFIC images.

Contrast is measured as the difference in signal intensities between two tissues of interest that have to be differentiated. This is usually measured as a percent difference relative to one of the tissues:

$$Contrast = \left(\frac{signal_1 - signal_2}{signal_1} \right) \times 100 \text{ (in percent)} \quad [6]$$

Since the ability to distinguish between different signal intensities is affected by the noise in an image, a better criterion for choosing the image with optimum contrast is the ratio of the signal intensity difference to that of the SD of noise:

$$CNR = \left(\frac{signal_1 - signal_2}{\sigma_{noise}} \right) \quad [7]$$

The two sources of signals used in Eqs. [6] and [7] were the GM in the cortex and the most prominent WM structure in the brain, the corpus callosum.

Table 1
Transverse Relaxation Times and Contrast Measurements for the Formalin-Fixed Brain at for TE = 10 ms, and the Actively Stained Brain for TE = 4, 5, and 7 ms

	Formalin (TE = 10 ms)	Formalin + ProHance (TE = 4 ms)	Formalin + ProHance (TE = 5 ms)	Formalin + ProHance (TE = 7 ms)
CSF T_2	35.82 ± 1.48	18.08 ± 0.65	17.56 ± 0.92	14.44 ± 1.98
GM T_2	30.07 ± 1.59	15.54 ± 1.24	14.79 ± 0.58	11.98 ± 0.57
WM T_2	23.95 ± 1.24	13.91 ± 1.10	13.55 ± 0.54	10.06 ± 0.37
GM/WM contrast in MEFIC-16 image	26	141	92	40

RESULTS

T_2 Relaxation Measurement

Figure 2 shows 16 echo images of one slice in the coronal plane through the midbrain region from a 3D multiecho acquisition. The in-plane resolution is 86 μ with a slice thickness of 172 μ. The T_1 of the actively stained brain is <100 ms, vs. approximately 800 ms in the formalin-fixed brain. Thus at TR = 400 ms in the actively stained brain, the earlier echoes show high signal intensity depicting the proton density-weighted contrast. The latter echoes are T_2-weighted with a successive decrease in signal, but an increase in contrast between structures with different T_2 relaxation rates. Note that the laminar structure of the cortex is more evident at longer TEs. T_2 values obtained in actively-stained mouse brains for all three sets of acquisition parameters were compared with those previously computed for formalin-fixed brains. Table 1 illustrates that the T_2s of the actively stained specimens were roughly half those of the fixed specimen without ProHance. The table also shows a successive decrease in the T_2 relaxation times with an increase in interecho spacing for the actively stained specimens. Finally, it shows an increase in CNR in the presence of ProHance for the MEFIC-16 images, but a successive decrease in CNR as the interecho time increases.

SNR, CNR, and Contrast Measurement in MEFIC Data

Figure 3a shows the resultant MEFIC-16 T_2-weighted image of the slice in Fig. 2. Figure 3b shows a myelin-stained histology slide (Harvard mouse brain atlas) at the same coronal level in the brain. There is good correspondence between the two.

Figure 4 illustrates the relative contrast, CNR, and SNR for the different MEFIC data sets. The first observation is that the contrast, CNR, and SNR are all higher in the eighth echo of the multiecho acquisition compared to the single-echo acquisition at the same TE. This highlights the advantage of the multiecho CPMG over single-echo acquisitions for reducing susceptibility-induced dephasing. The next observation is that SNR in the MEFIC images, except MEFIC-8, is much greater than both the single-echo acquisition and the eighth-echo image from the multiecho acquisition. However, the contrast percentage decreases as the number of constituent images that make the MEFIC image is increased to include more echoes. The contrast between GM and WM decreases from 57% in Fig. 4c to 30% in Fig. 4f because the latter echoes incorporate more of the T_2 weighting of the CMPG sequence in the resultant MEFIC image. However, the SNR increases successively as we look at the measurements in Fig. 4c–f. As a result, the CNR, which incorporates both of these effects, increases from 10 in the image set computed from only the last eight echoes (Fig. 4c) to 92 in the image set computed from all 16 echoes (Fig. 4f). In this way, we have traded some of that SNR for enhanced contrast. Choosing the MEFIC image with 15 echoes gives a CNR between GM and WM of 74, and an average SNR of 282. Both of these values are much higher than those of the conventional T_2-weighted image in Fig. 4a and b, and provide the enhanced T_2-weighted contrast and required SNR for structure differentiation.

To illustrate the inverse relationship between the contrast and SNR of the MEFIC images further, Fig. 5 presents the same coronal slice from four different reconstructions of a 16-echo 3D acquisition. The in-plane resolution for this acquisition was 43 μ with a slice thickness of 86 μ. A number of different structures can be visually evaluated here for the purpose of contrast analysis. In Fig. 5a the last eight echoes were used for reconstruction. The first structure that stands out is the dentate gyrus (DG) area of the hippocampus, which is well differentiated from the surrounding regions in the MEFIC-8 image. This stark definition in its appearance decreases in Fig. 5a–d. Next, the appearance of the medial geniculate nuclei (MG) in the midbrain region is diminished in the MEFIC-8 (Fig. 5a) image due to the loss in SNR. The best possible characterization of the MG is seen in MEFIC-14 (Fig. 5b) and MEFIC-15 (Fig. 5c). A third observation made here is that

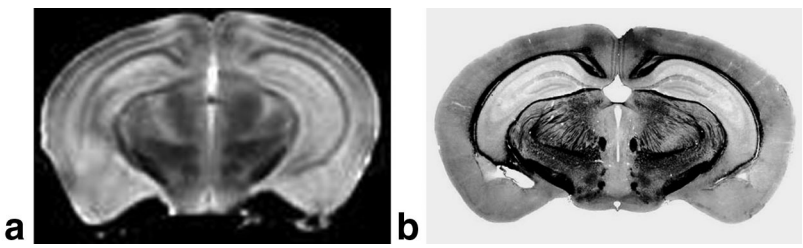

FIG. 3. **a:** T_2-weighted MEFIC image of the 16 echo images in Fig. 2 demonstrates good correspondence with (**b**) a corresponding myelin stain histology slide.

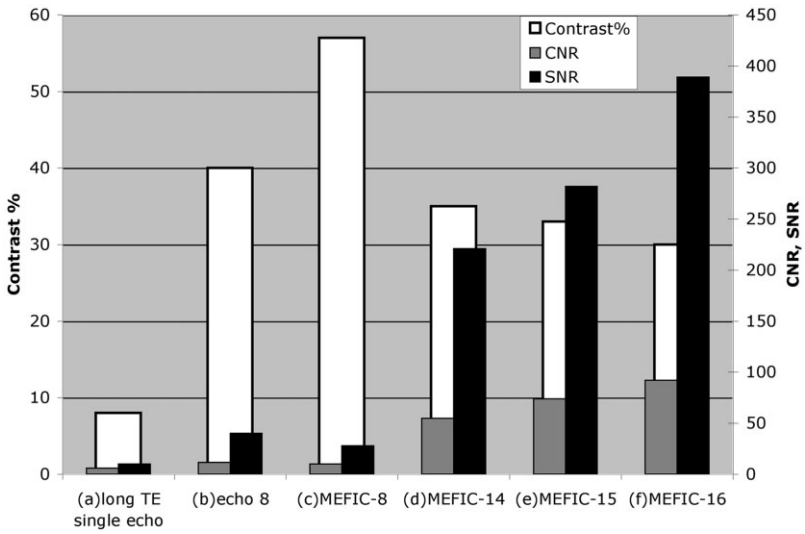

FIG. 4. Contrast, CNR, and SNR measurements are compared for different sources of T_2-weighted contrast: (**a**) single echo at TE = 40 ms, (**b**) echo 8 at TE = 40 ms, (**c**) T_2 MEFIC image reconstructed from the last eight echoes, (**d**) T_2 MEFIC image reconstructed from the last 14 echoes, (**e**) T_2 MEFIC image reconstructed from the last 15 echoes, and (**f**) T_2 MEFIC image reconstructed from all 16 echoes.

the boundaries of the corpus callosum (CC), which are well defined in MEFIC-14 through MEFIC-16, are blurry in MEFIC-8 due to the elevated noise in this image. The MEFIC-8 image is more T_2-weighted than the other data sets. The DG structure may be well defined in Fig. 5a because it requires a strongly T_2-weighted contrast to be differentiated from neighboring structures. These requirements vary from structure to structure. A more rigorous study for desired structures can be carried out to choose the optimum number of later echo images that should be used, depending on the CNR and SNR achievable with the given scan parameters.

R3.2 Figure 6 illustrates an example of how the image acquisition and processing scheme in this work can increase the accuracy of neuromorphometry studies in the mouse brain. It compares an image from a conventional 3D T_2 -weighted acquisition used in our initial attempt to perform automated segmentation for morphometry (19) and an image from the combined use of the 3D CPMG acquisition and the MEFIC postprocessing. Figure 6a is a slice from a large-flip-angle 3D T_2-weighted acquisition (FOV = 12 × 12 × 24, matrix = 128 × 128 × 256, TR = 400 ms, TE = 30 ms, flip angle = 135°, NEX = 2) of a formalin-fixed mouse brain with a histogram from an ROI. Figure 6b is a homologous slice in the MEFIC-16 T_2-weighted data set from a 3D CPMG acquisition (FOV = 12 × 12 × 24 mm, matrix = 256 × 256 × 512, TR = 400 ms, TE = 7, 14, 21, . . ., 112 ms, NEX = 1) with a histogram of a similar ROI. The ROI encloses the boundary between two structures of the striatum in the brain: the caudate putamen (CPU) and the globus pallidus (GP). The enclosed ROI is the same size in both cases. The total number of voxels is higher in the histogram of Fig. 6b because of the higher resolution of this data set. The intensity histogram in Fig. 6a is skewed and does not show a clear demarcation of the two structures because of overlapping intensity levels. However, the histogram in Fig. 6b is clearly bimodal and gives a clear demarcation of the boundary. This demonstrates the increased efficacy of the combined 3D CPMG acquisition and MEFIC processing for discriminating structures, which is a prerequisite for MR neuromorphometry.

Structure Identification in Isotropic 43-μ MEFIC T_2-Weighted Images

The collages in Figs. 7 and 8 show horizontal and coronal slices, respectively, from different anatomical regions in

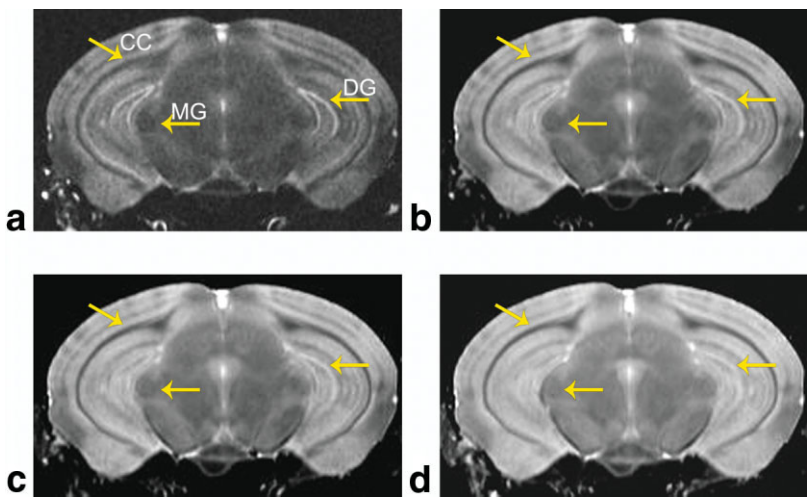

FIG. 5. T_2-weighted images reconstructed from the last eight echoes (**a**), last 14 echoes (**b**), last 15 echoes (**c**), and all 16 echoes (**d**). The contrast of the corpus callosum (CC), dentate gyrus (DG), and medial geniculate nucleus (MG) varies as the number of echoes used in the MEFIC T_2-weighted image is modified. Imaging parameters: FOV = 11 × 11 × 22, matrix = 256 × 256 × 256, TE = 5, 10, 15, . . ., 80 ms., TR = 400 ms.

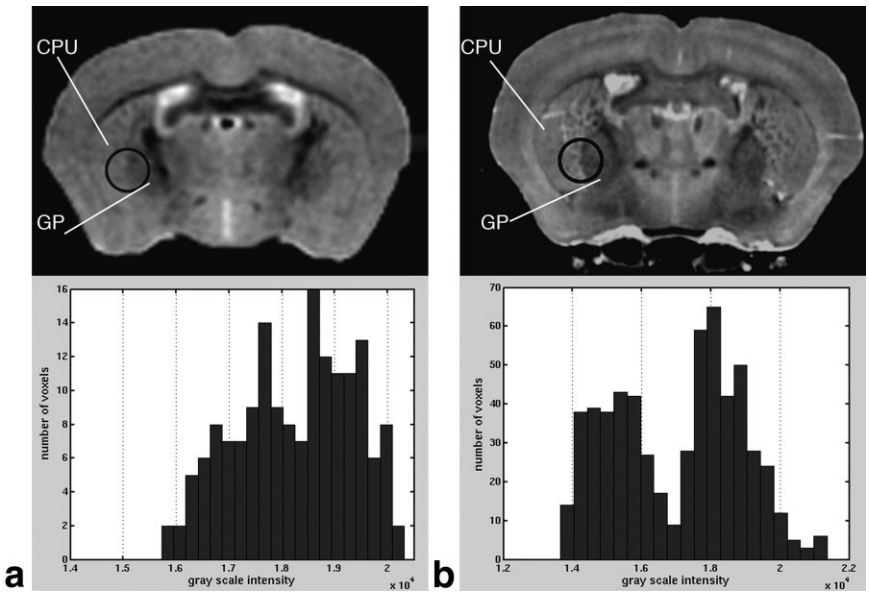

FIG. 6. Intensity histograms of selected ROI in formalin-fixed mouse brain with (**a**) a T_2-weighted sequence (FOV = 12 × 12 × 24, matrix = 128 × 128 × 256, TE = 30 ms, TR = 400 ms, flip angle = 135°) and (**b**) in actively-stained mouse brain with the 3D CPMG acquisition (FOV = 12 × 12 × 24 mm, matrix = 256 × 256 × 512, TR = 400 ms, TE = 7, 14, 21, . . ., 112 ms) and MEFIC postprocessing. The ROI encloses the boundary between two structures in the striatum: the caudate putamen (CPU) and the globus pallidus (GP). The area is the same in both cases. The CPMG-MEFIC combination in the actively-stained mouse brain shows a bimodal intensity distribution with clear boundaries between the structures.

the brain from a 3D MEFIC-16 image set. This data set was acquired with an FOV of 22 mm × 11 mm × 11 mm and a matrix size of 512 × 256 × 256, resulting in an isotropic resolution of 43 μ. The top panel in Fig. 7 is a horizontal slice toward the dorsal end of the brain, with a clear demarcation between the superior and inferior colliculi.

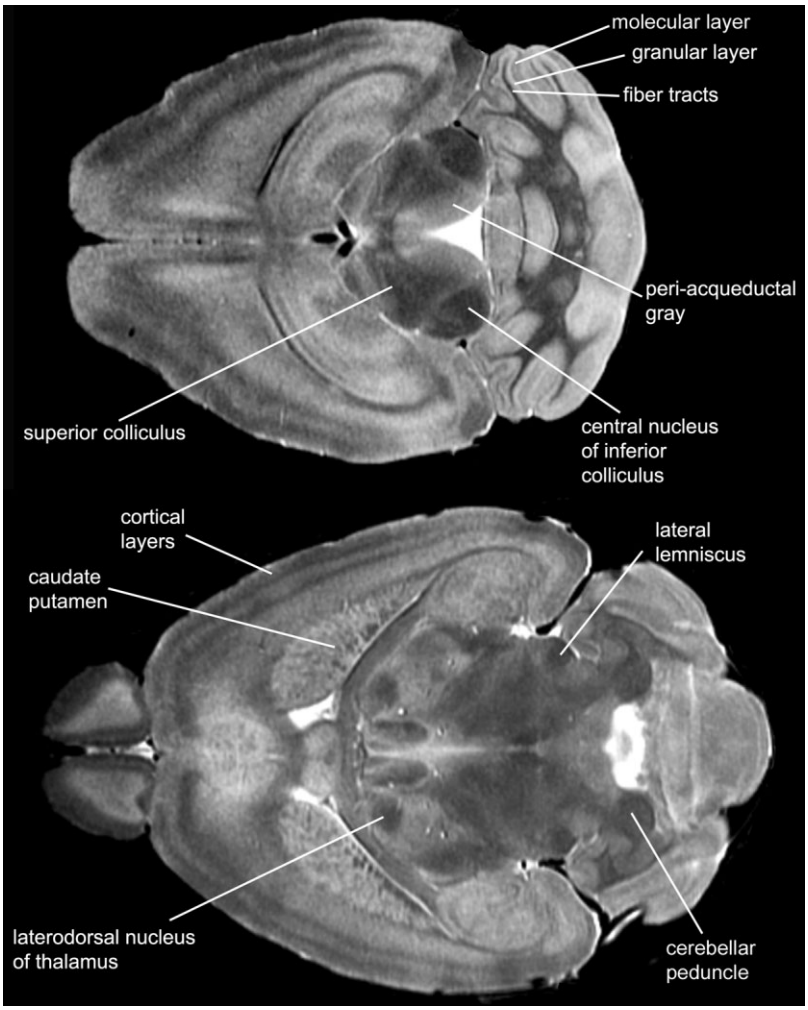

FIG. 7. Horizontal slices from a T_2-weighted, 43-μ, isotropic resolution acquisition of an actively-stained mouse brain demonstrate signal differences between WM structures of varied myelin content. Imaging parameters: FOV = 11 × 11 × 22, matrix = 256 × 256 × 512, TE = 7, 14, 21, . . .,112 ms., TR = 400 ms.

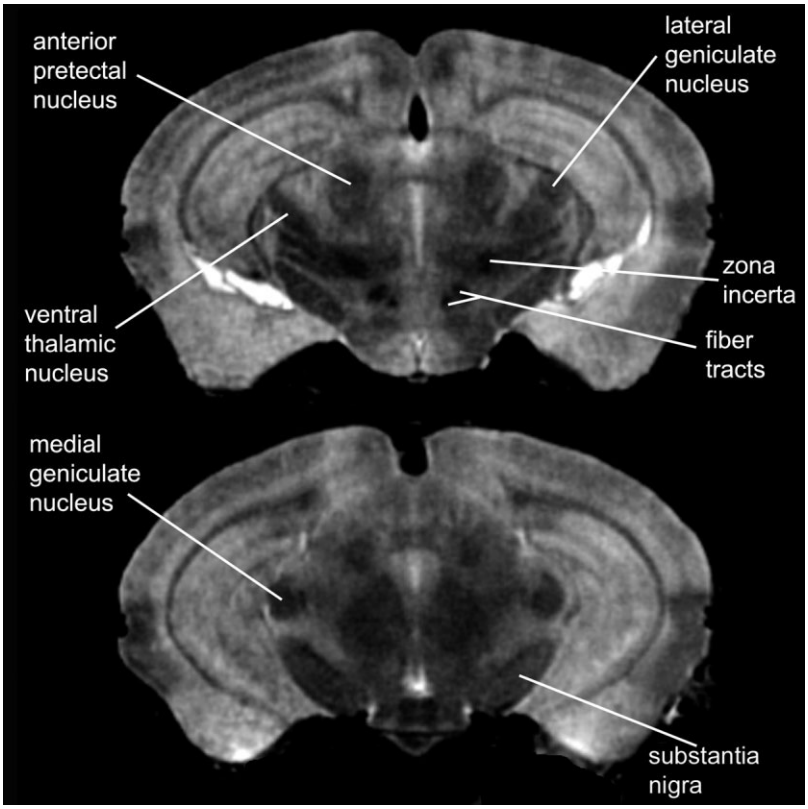

FIG. 8. Coronal slices from a T_2-weighted 43-μ isotropic resolution acquisition of an actively-stained mouse brain show a number of nuclei. Top: thalamus; bottom: midbrain. Imaging parameters: FOV = 11 × 11 × 22, matrix = 256 × 256 × 512, TE = 7, 14, 21, . . ., 112 ms., TR = 400 ms.

The central nucleus of the inferior colliculus has been labeled. We can also identify the multilayered regions of the superior colliculus. This particular slice demonstrates the intermediate layer and deep gray layer. Also seen distinctly are the molecular layer, granular layer, and the fiber tract layer of the cerebellum. The bottom panel is a horizontal slice situated ventrally. Identified here in detail are the laterodorsal nucleus of the thalamus, the lateral lemniscus, the cerebellar peduncles, the fiber structure of the caudate putamen, and at least five different layers of the cortex. Here the layers that are hypointense have shorter T_2s, probably due to a higher concentration of myelinated fibers (WM) than the layers that are hyperintense. Figure 8 shows coronal slices through the thalamus (top) and midbrain (bottom) regions of the brain. The top panel identifies several nuclei of the thalamus. The lateral geniculate nucleus, anterior pretectal nucleus, ventral thalamic nucleus, and zona incerta regions are well defined. Also seen are fiber tracts that go from the mammillary bodies to the thalamus. The thalamus is highly myelinated because it serves as the relay station for auditory, visual, and motor information to and from the cortex. The bottom panel in Fig. 8 distinctly shows the medial geniculate nucleus of the midbrain.

DISCUSSION

The results presented in this work demonstrate that the application of the MEFIC method to obtain T_2-weighted contrast in the actively-stained mouse brain has significant advantages with regard to SNR and CNR (Fig. 4). T_2-weighted contrast in the actively-stained mouse brain at 9.4 T is especially challenging due to paramagnetic contrast agent-induced susceptibility and gradient-induced diffusion losses. The MEFIC method enables us to regain the lost signal at long TEs while retaining T_2-weighted contrast. It gives us the flexibility to alter the contrast by modifying the number of echoes used in the computation (Fig. 5). This can accentuate specific structures of interest in morphometric studies. We demonstrated an improved demarcation between the globus pallidus and the caudate in the striatum of the actively-stained brain compared to conventional T_2-weighted acquisitions in the formalin-fixed brain (Fig. 6). We also observed an improved definition of the cortical layers, thalamic nuclei, superior colliculus layers, and cerebellum using the current acquisition and postprocessing scheme (Figs. 7 and 8). The MEFIC images demonstrate significant discrimination between predominantly myelinated and partially myelinated regions. The increased SNR provided by the MEFIC method obviates the need for averaging over multiple acquisitions, and thus reduces scan time. This will have a tremendous impact on MRH applications in which high-throughput screening of mice, in terms of both image acquisition and analysis, is a necessity.

The use of well-balanced crusher and imaging gradients, and short interecho spacing in the 3D CPMG sequence can reduce susceptibility- and gradient-induced diffusion, thereby suppressing stimulated-echo artifacts, and harness the signal up to the late-echo images indicative of T_2-weighted contrast. The TE may have to be relaxed to some extent depending on the resolution required. As the interecho spacing increases, there is a reduction in T_2 and a decrease in T_2-weighted contrast in the MEFIC image. The

number of echoes used in the MEFIC computation can be altered, and the value that gives the maximum overall contrast among all structures or a selected group in the area of interest should be chosen. Zhang et al. (16) employed a technique similar to the MEFIC method; however, instead of applying an FT in the echo dimension, they added four echo images acquired in four separate acquisitions with different TEs. Their resultant T_2-weighted images showed GM/WM contrast, but details such as the cortical layers and thalamic nuclei were not visible. Their acquisition times ranged from 8 to 24 hr depending on the desired resolution.

CONCLUSIONS

The use of active staining has revolutionized the field of MRH, enabling the acquisition of high-resolution data in reasonable scan times. In the past, MR contrast in the actively-stained mouse brain was limited mainly to T_1-weighted contrast. T_2-weighted acquisitions posed great challenges due to the decaying signal at long TEs and the long scan times involved. The decay arises in part from spin dephasing induced by diffusion through susceptibility-induced gradients. With the combined implementation of short interecho spacing in the 3D CPMG sequence and the multiecho frequency domain image contrast method, we were able to obtain enhanced T_2-weighted contrast in the actively-stained mouse brain at 9.4 T. We achieved isotropic 43-μ resolution in a scan time of 4 hr. The resultant T_2-weighted images characterize the myeloarchitecture and cytoarchitecture of the mouse brain in exquisite detail, which makes this an invaluable source of contrast for future studies of automated segmentation and morphometry in the mouse brain.

ACKNOWLEDGMENTS

The authors thank Boma Fubara for specimen preparation and valuable insight into mouse neuroanatomy. All work was performed at the Duke Center for In Vivo Microscopy, an NIH/NCRR National Biomedical Technology Resource Center and in collaboration with the Mouse Bioinformatics Research Network (NIH/NCRR, grant U24 RR021760).

REFERENCES

1. Johnson GA, Benveniste H, Black RD, Hedlund LW, Maronpot RR, Smith BR. Histology by magnetic resonance microscopy. Magn Reson Q 1993;9:1–30.
2. Johnson GA, Cofer GP, Gewalt SL, Hedlund LW. Morphologic phenotyping with magnetic resonance microscopy: the visible mouse. Radiology 2002;222:789–793.
3. Zhang J, Richards LJ, Yarowsky P, Huang H, van Zijl PCM, Mori S. Three dimensional anatomical characterization of developing mouse brain by diffusion tensor microimaging. Neuroimage 2003;20:1639–1648.
4. Hoult DI, Richards RE. The signal to noise ratio of the nuclear magnetic resonance experiment. J Magn Reson 1976;24:71–85.
5. Hart HR, Bottomley PA, Edelstein WA, Karr SG, Leue WM, Mueller O, Redington RW, Schenck JF, Smith LS, Vatis D. Nuclear magnetic resonance imaging: contrast-to-noise ratio as a function of strength of magnetic field. AJR Am J Roentgenol 1983;141:1195–1201.
6. Wehrli FW, MacFall JR, Glover GH, Grigsby N, Haughton V, Johansen J. The dependence of nuclear magnetic resonance (NMR) imaging contrast on intrinsic and pulse sequence timing parameters. Magn Reson Imaging 1984;2:3–16.
7. Bottomley PA, Foster TH, Argersinger RE, Pfeifer LM. A review of normal tissue hydrogen NMR relaxation times and relaxation mechanisms from 1–100 MHz: dependence on tissue type, NMR frequency, temperature, species, excision, and age. Med Phys 1984;11:425–448.
8. Johnson GA, Herfkens RJ, Brown MA. Tissue relaxation time: *in vivo* field dependence. Radiology 1985;156:805–810.
9. Dockery SE, Suddarth SA, Johnson GA. Relaxation measurements at 300 MHz using MR microscopy. Magn Reson Med 1989;11:182–192.
10. Callaghan PT. Principles of nuclear magnetic resonance microscopy. Oxford: Oxford University Press; 1994. 516 p.
11. Cremillieux Y, Ding S, Dunn JF. High-resolution in vivo measurements of transverse relaxation times in rats at 7T. Magn Reson Med 1998;39:285–190.
12. Guilfoyle DN, Dyakin VV, O'Shea J, Pell GS, Helpern JA. Quantitative measurements of proton spin-lattice (T1) and spin-spin (T2) relaxation times in the mouse brain at 7T. Magn Reson Med 2003;49:576–580.
13. Sun Y, Mulkern RV, Schmidt K, Doshi S, Albert MS, Schmidt NO, Ziu M, Black P, Carrol R, Kieran MW. Quantification of water diffusion and relaxation times of human U87 tumors in a mouse model. NMR Biomed 2004;17:399–404.
14. van Dorsten FA, Olah L, Schwindt W, Grune M, Uhlenkuken U, Pillekamp F, Hossmann KA, Hoehn M. Dynamic changes of ADC, perfusion, and NMR relaxation parameters in transient focal ischemia of rat brain. Magn Reson Med 2002;47:97–104.
15. Degaonkar MN, Raghunathan P, Jayasundar R, Jagannathan NR. Determination of relaxation characteristics during preacute stage of lysophosphatidyl choline-induced demyelinating lesion in rat brain: an animal model of multiple sclerosis. Magn Reson Imaging 2005;23:69–73.
16. Zhang J, Yarowsky P, Gordon MN, Di Carlo G, Munireddy S, vanZijl PCM, Mori S. Detection of amyloid plaques in mouse models of Alzheimer's disease by magnetic resonance imaging. Magn Reson Med 2004;51:452–457.
17. Redwine JM, Kosofsky B, Jacobs RE, Games D, Reilly JF, Morrison JH, Young WG, Bloom FE. Dentate gyrus volume is reduced before onset of plaque formation in PDAPP mice: a magnetic resonance microscopy and stereologic analysis. Proc Natl Acad Sci USA 2003;100:1381–1386.
18. Kovacevic N, Henderson JT, Chan E, Lifshitz N, Bishop J, Evans AC, Henkelman MR, Chen XJ. A three-dimensional MRI atlas of the mouse brain with estimates of the average and variability. Cereb Cortex 2005;15:639–645.
19. Ali AA, Dale AM, Badea A, Johnson GA. Automated segmentation of neuroanatomical structures in multispectral MR microscopy of the mouse brain. Neuroimage 2005;27:425–435.
20. Yang QX, Demeure RJ, Dardzinski BJ, Arnold BW, Smith MB. Multiple echo frequency-domain image contrast: improved signal-to-noise ratio and T2(T2*) weighting. Magn Reson Med 1999;41:423–428.
21. Carr HY, Purcell EM. Effects of diffusion on free precession in nuclear magnetic resonance experiments. Phys Rev 1954;94:630.
22. Meiboom S, Gill D. Modified spin-echo method for measuring nuclear relaxation times. Rev Sci Instrum 1958;29:688–691.
23. Majumdar S, Gore JC. Studies of diffusion in random fields produced by variations in susceptibility. J Magn Reson 1988;78:41–55.
24. Majumdar S, Orphanoudakis SC, Gmitro A, Donnell MO, Gore JC. Errors in the measurements of T2 using multiple-echo MRI techniques. I. Effects of radiofrequency pulse imperfections. Magn Reson Med 1986;3:397–417.
25. Crawley AP, Henkelman RM. Errors in T2 estimation using multislice multiple-echo imaging. Magn Reson Med 1987;4:34–47.
26. Zur Y, Zou X, Neuringer LJ. Multiecho, spin-echo sequence to eliminate unwanted echoes. Magn Reson Med 1991;19:464–469.
27. Poon CS, Henkelman RM. Practical T2 quantitation for clinical applications. J Magn Reson Imaging 1992;2:541–553.
28. Levitt MH, Freeman R. NMR population inversion using a composite pulse. J Magn Reson 1979;33:473.